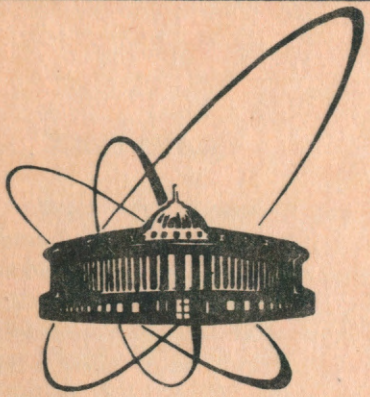

сообщения
объединенного
института
ядерных
исследований
дубна

E1-91-230

B.Słowiński

# EXPERIMENTAL INVESTIGATION OF ELECTROMAGNETIC SHOWERS PRODUCED IN LIQUID XENON BY GAMMA QUANTA BETWEEN 100 AND 3500 MeV

1991

Словинский Б. E1-91-230

Экспериментальное исследование электромагнитных ливней, инициируемых в жидком ксеноне гамма-квантами с энергией от 100 до 3500 МэВ

Изучены основные характеристики электромагнитных ливней, вызываемых гамма-квантами с энергией 100÷3500 МеВ/с, зарегистрированных на снимках 180-литровой ксеноновой пузырьковой камеры ИТЭФ /Москва/: продольное и поперечное развитие, их взаимные корреляции и флуктуации. Получены формулы, описывающие соответствующие профили ливней и флуктуации в виде скейлинга относительно первичной энергии и среды.

Работа выполнена в Лаборатории высоких энергий ОИЯИ и в Институте физики Варшавского Технического Университета.

Сообщение Объединенного института ядерных исследований. Дубна 1991

Słowiński B. E1-91-230

Experimental Investigation of Electromagnetic Showers Produced in Luquid Xenon by Gamma Quanta between 100 and 3500 MeV

Extensive experimental studies of main characteristics of electromagnetic showers produced by gamma-quanta of 100-3500 MeV using pictures of the 180 l xenon bubble chamber of ITEP (Moscow) have been carried out. Investigated are the longitudinal and lateral development, as well as their mutual correlations and fluctuations. The obtained parametrization of the relevant shower profiles and fluctuations display a simple scalling with the primary energy and the material used.

The investigation has been performed at the Laboratory of High Energies, JINR and at the Institute of Physics of the Warsaw University of Technology.

Communication of the Joint Institute for Nuclear Research. Dubna 1991

## 1. INTRODUCTION

Many experimental results about electromagnetic showers produced by high-energy gamma-quanta (GQ) in dense enough media have been obtained by now using various methods and techniques since the phenomenon was first discovered[1]. Most of these results concern the longitudinal or lateral profiles of showers mainly in order to be used for the identification and energy determination of photons in shower detectors of several concrete forms, as well as for some dosimetric purposes. Nevertheless, scarce experimental information is available on such important shower characteristics as fluctuations and correlations. On the other hand, the EGS4 Code System[2] considered to be a universal and adequate approach to the problem requires a large amount of time of big computers, although the one- and three-dimensional parametrizations of average shower profiles were suggested[3,4] and further improvements of shower simulation methods were elaborated[5-7]. Meanwhile, for many practical purposes a compact and, as far as possible, quantitative information on main characteristics of showers is necessary.

In this paper we report on an extensive and systematic experimental study of longitudinal and lateral development of electromagnetic showers created by GQ of 100-3500 MeV using pictures of the 180 liter xenon bubble chamber (XeBC) of ITEP (Moscow)[8]. The major advantages of the liquid xenon for this work are that it has a short radiation length (rl), $\ell_{Xe}$ = 4.05±0.17 cm[9] as measured in the 24 liter XeBC of JINR*, and provides an acceptably clear image of tracks of electrons with the energy not less than 0.5-1.5 MeV. Large enough dimensions of the 180$\ell$ XeBC expressed in units of rl, 25.7x11x10 $rl^3$ enable one to measure practically all ranges of shower electrons and positrons (later: electrons) registered in a picture plane (PP). So, it turns out available a thorough investigation

* This value is somewhat larger than the similar one quoted in literature[1,10] because of addition of ethylene (0.5% by weight) for quenching of scintillation.

of such complicated process without any substantial distortion caused by the detector except, may be, a relatively small region of length $\Delta t = 2r1$ along the shower axis (SA), and of thickness $\Delta p = 0.25r1$, around the shower maximum near by the SA at higher energies of primary photons ($E_\gamma \geq 1500$ MeV) where the density of electrons becomes sometimes too large to separate some overlapping short electron tracks.

## II. MATERIAL AND METHOD

About 220 thousand pictures of the 180 XeBC exposed to the beam of $\pi^-$ mesons at 3.5 GeV/c were scanned twice at least, and 1657 events of showers satisfying the appropriate criteria were selected. In particular, these criteria assume that the SA of each event is in the PP of a picture and there are no other background showers or tracks on the picture. For each event chosen during the scanning the energy $E_\gamma$ of GQ initiating the shower was evaluated using the linear relation between $E_\gamma$ and the total range $\Sigma r_i$ of shower electrons measured in the PP[11]:

$$E_\gamma = a \Sigma r_i , \qquad (1)$$

where $a$ = 0.59 0.02 MeV/mm. The so-called potential length $L_{pot}$, as well as the maximum shower length $t_{max}$ were measured, too. These lengths were counted out from the conversion point of a photon initiating shower along the SA respectively up to the edge of the active volume of the XeBC ($L_{pot}$) and the remotest visible tracks of shower electrons (t). Then all selected events were grouped into 22 intervals of primary

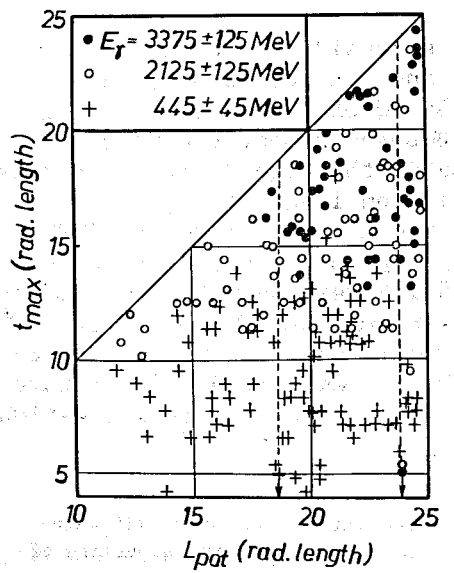


Fig.1. Scatter plot of potential lengths $L_{pot}$ vs maximum visible shower lengths t for the selected events to showers produced by photons of energy $E_\gamma$.



photon energy $E_\gamma$ so that half the relative width $\Delta E_\gamma / E_\gamma$ of these intervals might be roughly equal to the average energy resolution in the XeBC, e.g. ~ 0.1[12]. To reduce the effect caused by the limited dimensions of the registering volume of the XeBC used in the work ($\lesssim 25.7r1$), the scatter plots ($L_{pot}$ vs t) for all intervals were examined. Figure 1 shows such plots for three of these intervals. Supposing our sample of events to be represantative enough, one can expect that the showers satisfying the evident condition

$$L_{pot}(E_\gamma) \leq t_{max}(E_\gamma) \qquad (2)$$

are unbiased as far as possible. Here $t_{max}(E_\gamma)$ is the maximum value of t in the sample of events belonging to a given interval of primary photon energy centered at $E_\gamma$.

The numbers $N_\gamma$ of selected events of showers falling to each interval of energy $E_\gamma$ and the average values $\bar{E}_\gamma$ of $E_\gamma$ in these intervals are given in table 1. The values of $t_{max}(E_\gamma)$ and the numbers $N^*_\gamma$ of events fulfilling the condition (2) are presented there, too.

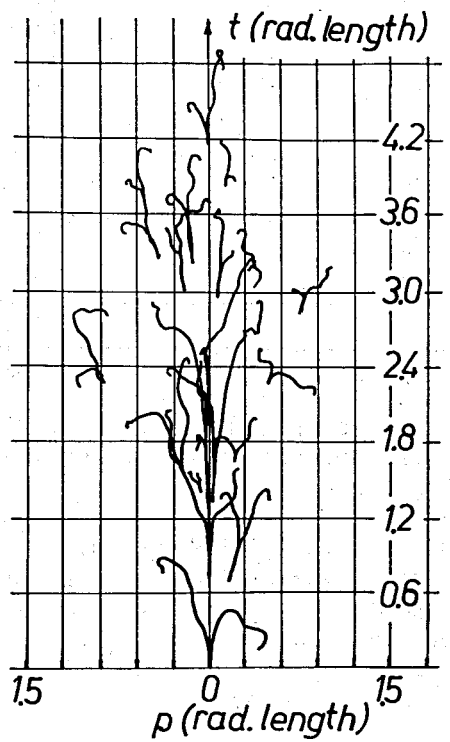


Fig.2. Schematic outline of a shower recorded on a picture of the xenon bubble chamber and the grid used in the work to measure plane projection ranges of shower electrons.

So, among 1657 events of showers selected in the scanning and satisfying the basic criteria only 908 passed the condition (2) and were used for furtfer analysis which has been carried out on the PP at an average enlargement of about 0.94 using grid with the dimensions of the elementary square $\Delta t = 0.6r1$ along the SA and $\Delta p = 0.3$ r1 in its transversal direction, as shown in fig.2. For every event summary plane projection ranges of shower electrons (SER), $\Delta \Sigma r_i (E_\gamma, t, p)$, were measured

Table 1. Numbers $N_\gamma$ of selected events of showers produced by GQ with the energy $E_\gamma$. $N^*_\gamma$ is the number of events satisfying the condition (2). $\bar{E}_\gamma$ is the mean energy of the relevant interval

| $E_\gamma \pm \Delta E_\gamma$ (MeV) | $\bar{E}_\gamma$ (MeV) | $N_\gamma$ | $t_{max}(E_\gamma)$, rl | $N^*_\gamma$ |
|---|---|---|---|---|
| 3375 ± 125 | 3489 ± 35 | 46 | 24.0 | 15 |
| 3125 ± 125 | 3139 ± 18 | 42 | 24.0 | 12 |
| 2875 ± 125 | 2850 ± 17 | 41 | 24.0 | 11 |
| 2625 ± 125 | 2599 ± 25 | 53 | 22.6 | 12 |
| 2375 ± 125 | 2373 ± 16 | 60 | 22.6 | 20 |
| 2125 ± 125 | 2117 ± 15 | 63 | 21.3 | 35 |
| 1875 ± 125 | 1864 ± 12 | 80 | 20.5 | 33 |
| 1625 ± 125 | 1615 ± 9 | 108 | 20.0 | 66 |
| 1375 ± 125 | 1363 ± 10 | 129 | 20.0 | 58 |
| 1125 ± 125 | 1116 ± 8 | 158 | 20.0 | 80 |
| 875 ± 125 | 871 ± 8 | 204 | 20.0 | 86 |
| 680 ± 70 | 677 ± 5 | 138 | 20.0 | 60 |
| 555 ± 55 | 555 ± 4 | 108 | 20.0 | 58 |
| 455 ± 45 | 459 ± 3 | 103 | 18.6 | 59 |
| 375 ± 35 | 380 ± 3 | 65 | 17.3 | 61 |
| 310 ± 30 | 309 ± 2 | 58 | 16.0 | 53 |
| 255 ± 25 | 252 ± 2 | 55 | 14.9 | 55 |
| 210 ± 20 | 208 ± 2 | 49 | 14.8 | 47 |
| 175 ± 15 | 177 ± 2 | 29 | 12.6 | 29 |
| 145 ± 15 | 145 ± 2 | 24 | 12.6 | 24 |
| 120 ± 10 | 123 ± 2 | 21 | 11.6 | 20 |
| 100 ± 10 | 100 ± 1 | 23 | 11.0 | 14 |
| total | | 1657 | | 908 |

in each square of the grid when the axis p = 0 coincides with the SA and the origin coincides with the conversion point of a primary GQ producing shower (fig.2).

By means of the computer modeling of electron ranges in showers created in the XeBC by GQ of 100-3000 MeV it has been shown that the ratio $\eta(E_\gamma, t, p)$ of shower electron ionization loss (IL), $\Delta\Sigma E_e(E_\gamma, t, p)$, to relevant SER is constant within a few percent in the central shower region in which, on the average, more than 90% of the total energy $E_\gamma$ is released [12]. So, a more general relation than (2) can be written:



$$\frac{\Delta\Sigma E_e(E_\gamma, t, p)}{\Delta t \Delta p} = \eta(E_\gamma, t, p) \cdot \frac{\Delta\Sigma r_1(E_\gamma, t, p)}{\Delta t \Delta p}. \qquad (3)$$

It should be noted that within a small shower region in the immediate vicinity of the conversion point of primary photon, e.g., at $t \lesssim 0.5$rl and $p \lesssim 0.1$rl, where one observes mostly two straight tracks of high energy ($\sim E_\gamma/2$) electrons only and there is practically no cascading, the coefficient $\eta$ is by about 20% greater than its average value in all investigated interval of $E_\gamma$. Outside the aforesaid central region, where the shower fades, $\eta$ slowly decreases, too, by about 10-15% mainly along the SA and at higher energies ($E_\gamma \gtrsim 1000$ MeV). Besides, the coefficient $\eta$, averaged over all t and p within each interval of energy $E_\gamma$, does not depend on $E_\gamma$ [13]. So, one can admit that $\eta$ in eq.(3) is a constant value to the accuracy, on the average, of ~3%, as assumed in the work. Mention finally that the SER were measured with an average accuracy of about 20%, but at the end of a shower the error can reach even 50%.

## III. LONGITUDINAL PROFILE

Figure 3 shows the longitudinal distribution of average IL for six among 22 analysed in the work intervals of primary GQ energy $E_\gamma$ as a function of the ratio $t/\bar{t}(E_\gamma)$, where $\bar{t}(E_\gamma)$ is the estimate of the average value of shower depth t. The energy dependence of $\bar{t}(E_\gamma)$ is illustrated in Fig.4 and fitted to the linear function of $\ln E_\gamma$

$$\bar{t}(E_\gamma) = a_t + b_t \cdot \ln E_\gamma \qquad (4)$$

also shown in the figure as a solid line. Here $a_t = -4.84 \pm 0.09$ rl, $b_t = 1.32 \pm 0.03$ at the linear correlation index $r = 0.996$ ($E_\gamma$ is in MeV). One can notice that at $E_\gamma \gtrsim 500$ MeV the distribution becomes independent of the energy $E_\gamma$, within the error, except the very beginning of a shower, i.e., at $t/\bar{t}(E_\gamma) \lesssim 0.15$, where a strong descreasing of IL is observed when $E_\gamma$ increases. It is caused by the diminishing (as $\sim E_\gamma^{-1}$) of multiple scattering of electrons and positrons from the pairs created directly by primary photons while the relativistic increase of their IL whithin logarithmical rising $\bar{t}(E_\gamma)$ is about $\ln^2 E_\gamma$ only. (This tendency should be still much significant at very high energy, i.e., at $E_\gamma \gtrsim 100$ GeV, but this time owing to the Chudakov effect).

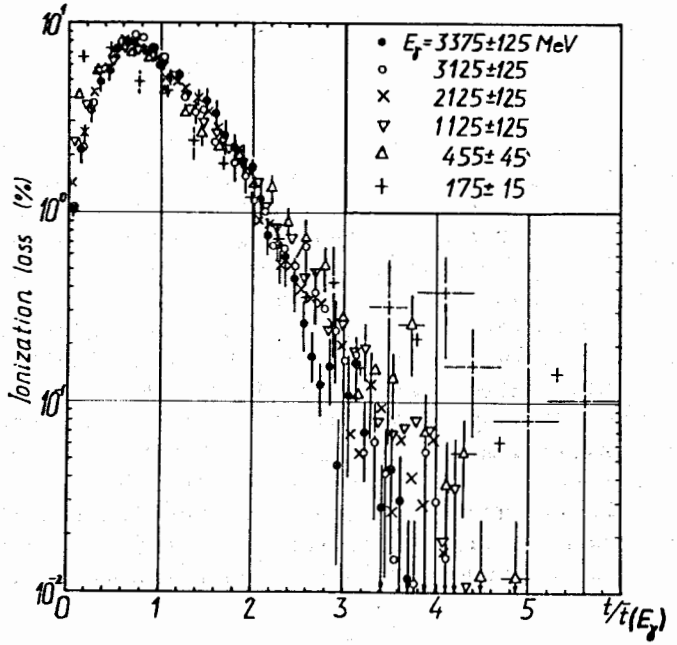


Fig.3. Longitudinal shower development as a function of the ratio $t/\bar{t}(E_\gamma)$ of the depth t and the average shower depth $\bar{t}(E_\gamma)$ at the energy $E_\gamma$.

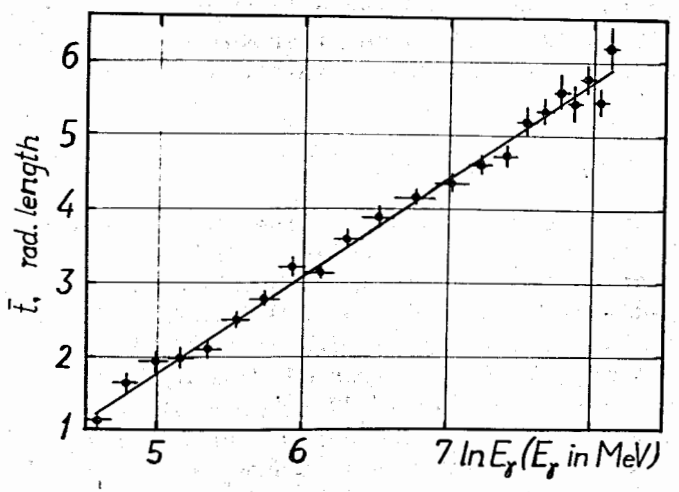


Fig.4. Average shower depth as a function of the primary photon energy $E_\gamma$. Superimposed is the fitting function (4).



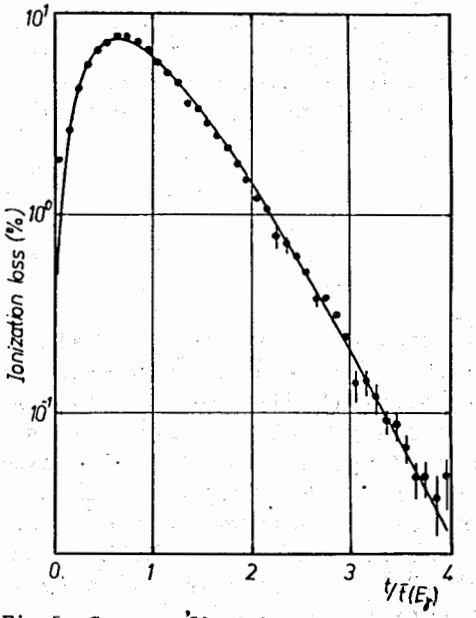


Fig.5. Same as fig.3 but averaged over the range of $E_\gamma$ = 500-3500 MeV.

Taking into account the above, the data at $E_\gamma \gtrsim 500$ MeV have been averaged and fitted to the function, normalized to 1:

$$F_t(x) = a_1 x^{a_2} \exp(-a_3 x), \qquad (5)$$

where $x = t/\bar{t}(E_\gamma)$ and $a_1 = 83.1\pm3.4$, $a_2 = 1.65\pm0.03$, $a_3 = 2.62\pm0.03$ at $\chi^2_{35} = 35.8$, when $x \gtrsim 0.15$. The experimental results and fitting function are presented in Fig.5.

One can conclude that the average shower depth $\bar{t}(E_\gamma)$ is a useful scaling parameter for concise and reliable enough description of the longitudinal distribution of IL at least in the region of not too high primary GQ energy.

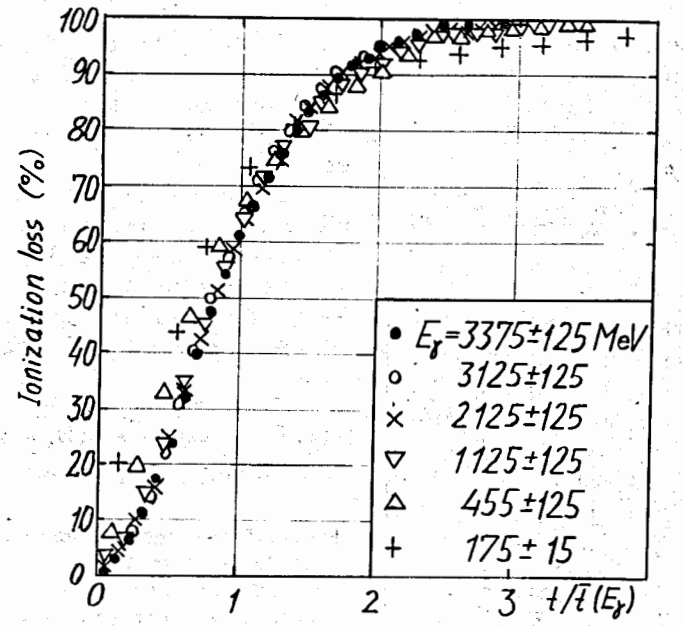


Fig.6 Same as fig.3 but for cumulative distribution.

Figure 6 shows the cumulative distribution of IL along the SA for the same as in Fig.3 values of energy $E_\gamma$. It may be seen from the figure that, for example, within the thickness of an absorbent equal to $\sim 2 \cdot \bar{t}(E_\gamma)$ more than 0.9 of the total shower energy is realized.

## IV. LATERAL PROFILE

### 1. Plane Distribution

As the 180 l XeBC used in the work enables one to obtain the experimental information about the lateral IL distribution in the PP, the relevant average radial IL distribution can be reconstructed taking into account the geometrical conditions of the showar electron ranges recording, as well as axial symmetry of the average IL around the SA [8,14]. In Fig.7, as an example, the lateral distribution of IL measured in the PP is histogrammed with bins of 1.2 rl along the SA for showers initiated by GQ of energy $E_\gamma$ = 1125±125 MeV. Experimental data are fitted to the exponential function

$$f_p(p|t, E_\gamma) = e^{-p/\bar{p}(t, E_\gamma)} / \bar{p}(t, E_\gamma) \qquad (6)$$

also presented in the figure as a dashed line. Here $\bar{p}(t, E_\gamma)$ is the average shower width at the shower depth t and a given value of $E_\gamma$. The fitted values of the parameter $\bar{p}(t, E_\gamma)$ are also shown in Figs.8a-8c for all 22 intervals of primary photon energy.

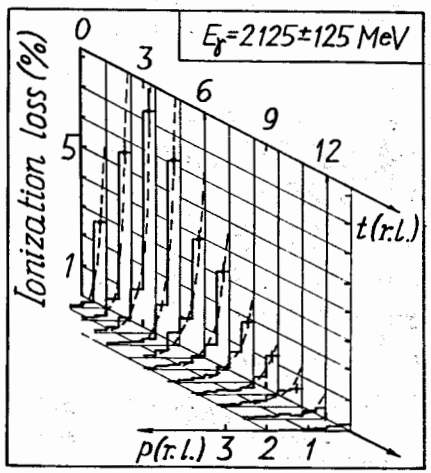


Fig.7. Plane lateral spread at different depths t of showers produced by photons of energy $E_\gamma$ = 1125 ±125 MeV. Dashed lines represent the best fit to the form (6).

As the displayed points are markedly collimated along some straight lines, at least at lower values of t, it is reasonable to approximate the t dependence of $\bar{p}$ to the linear function

$$\bar{p}(t, E_\gamma) = \alpha(E_\gamma) + \beta(E_\gamma) \cdot t, \qquad (7)$$



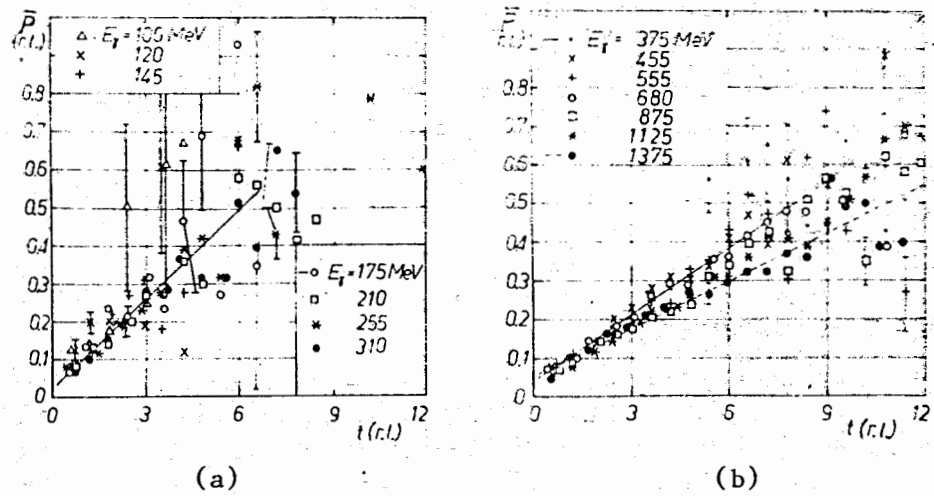


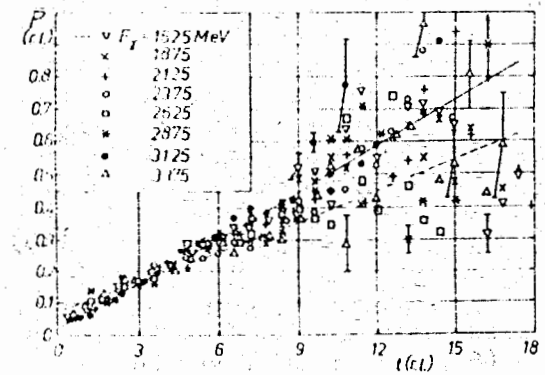


Fig.8. Dependence on t of the slope parameter $\bar{p}$ for a primary photon energy of: (a) 100-310 MeV, (b) 373-1375 MeV, (c) 1625-3375 MeV. The straight lines represent the linear function (7).

where $\alpha$ and $\beta$ may depend on the energy $E_\gamma$. But because of relatively low statistics of available shower events the spread of $\bar{p}$ increases with t increasing. That's why the parameters $\alpha$ and $\beta$ have been estimated for two t intervals: 0-6 rl, 0-12 rl and for all values of t. As a result we can conclude that the parameter $\alpha$ does not depend on $E_\gamma$ (within large enough errors) and is equal to

$$\alpha = 0.042 \pm 0.015 \text{ rl} \quad [15],$$

whereas the $E_\gamma$ dependence of $\beta$ can be represented by the formula:

$$\beta(E_\gamma) = c + d \cdot \ln E_\gamma, \qquad (8)$$

where the fitted values of the parameters c and d are given in table 2 for three intervals of t.

Table 2. Values of dimensionless parameters c and d appearing in eq.(8) at $E_\gamma \gtrsim 175$ MeV

| t (rl) | $c \cdot 10^3$ | $-d \cdot 10^4$ |
|---|---|---|
| 0 - 6 | 67 ± 4 | 53 ± 5 |
| 0 - 12 | 72 ± 3 | 62 ± 4 |
| all | 75 ± 3 | 66 ± 4 |

## 2. Radial Distribution

The average radial distribution of IL, $F_r(r, E_\gamma|t)$, is related with the relevant plane distribution $f_p(p|E_\gamma, t)$ measured in the experiment by means of the following equation [14]

$$f_p(p|E_\gamma, t) = 2 \cdot \int_p^\infty \frac{F_r(r, E_\gamma|t)\, dr}{\sqrt{1-(p/r)^2}} \quad . \tag{9}$$

In general, the solution of this equation is of the form [16]:

$$F_r(r, E_\gamma|t) = \frac{1}{\pi r^2} \int_\infty^r \frac{d}{dp}[p \cdot f_p(p|E_\gamma, t)] \cdot \frac{dp}{\sqrt{1-(r/p)^2}} . \tag{10}$$

Unfortunately, although the plane distribution $f_p(p|E_\gamma, t)$ is a simple exponential function (6), the radial distribution $F_r(r, E_\gamma|t)$ cannot be expressed in the so simple functional form but its numerical values can be easily obtained using the computer techniques. Nevertheless, the root-mean-square shower radius can be simply computed as [17] $\langle \bar{r}^2 \rangle^{1/2} = 2 \cdot \bar{p}$.

## V. SPATIAL SHOWER STRUCTURE

The three-dimensional distribution of average IL released within a ring of a volume $\Delta V = 2\pi r \Delta r \Delta t$ around the SA can then be described by

$$\frac{\Delta \Sigma E_e(E_\gamma, t, r)}{2\pi r \Delta r \Delta t} = E_\gamma \cdot F_t(t, E_\gamma) \cdot F_r(r, E_\gamma|t), \tag{11}$$

where the functions $F_t$ and $F_r$ are determined by the expressions (5) and (10), respectively. This distribution allows, for example, simple numerical estimation of the shower energy deposition within a given volume of a homogeneous and dense enough absorbent.



## VI. CORRELATIONS

### 1. Longitudinal-Lateral Spread

Figures 9 and 10 display scatter plots of IL in showers produced by GQ of energy $E_\gamma$ = 375 MeV and 3375 MeV, respectively, at fixed fraction A of the total IL equal to 0.9, 0.8, 0.7 and 0.6. Every marked point (t, p) on the diagrams means that between two parallel planes each perpendicular to the PP and separated a distance p from the SA on its both sides whereas the depth of an absorber, measured from the conversion point of a primary photon, is equal to t, the fraction A of the total IL is deposited. As any given value of A can be obtained by means of different sets of (t, p), the relevant points for some individual event may form the regular tracks, particularly vizualized at higher $E_\gamma$ and A close to 1 when fluctuations are not so important. Moreover, the collimation of (t, p) points increases with decreasing A, especially at higher $E_\gamma$, indicating that the main contribution to the fluctuations of IL is caused by the remotest low energy shower electrons. Besides, the lower is the fraction A the most collimated are the points round the average dependence of (t vs.p) shown in the figures by solid lines.

### 2. Average Longitudinal-Lateral Correlation

Figure 11 shows the estimates of the dependence between average values of the depth t and width p in the PP for showers produced by GQ at eight values of energy $E_\gamma$: 100, 175, 310, 455, 1125, 1625, 2625 and 3375 MeV. These results refer to four different values of the fraction A of the total IL deposited on an absorber volume limited to t along the SA and 2·p across it with the SA in the middle. Inspection of Fig.11 indicates that the probability of measuring energy of GQ with acceptable reliability increases significantly at large enough dimensions of a calorimeter, viz. at $t \gtrsim 15$ rl and $p \gtrsim 2$ rl.

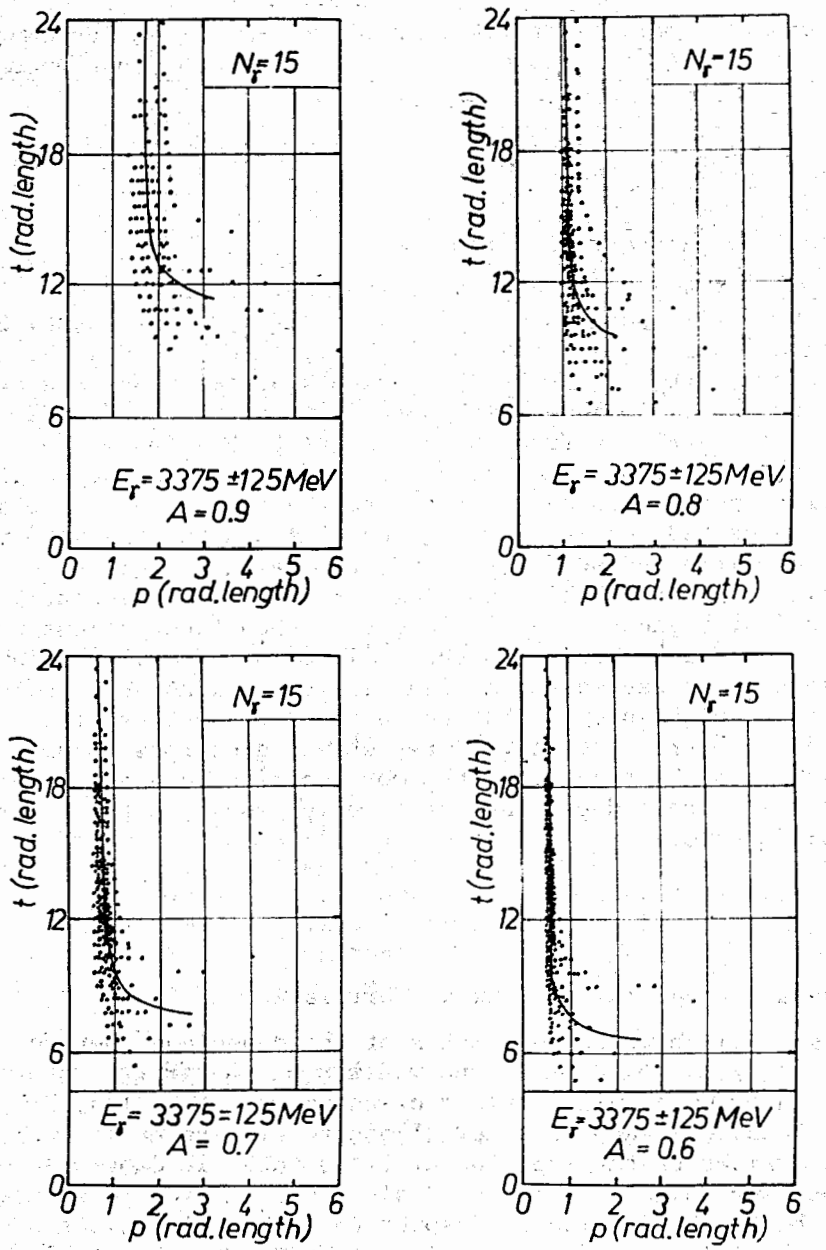


Fig.9. Scatter plots of points (t, p) at different values of the fraction A of the total IL for showers initiated by GQ of energy $E_\gamma$ = 3375 ± 125 MeV. Solid lines show the relevant t vs.p dependence averaged over all sample of $N_\gamma$ shower events.



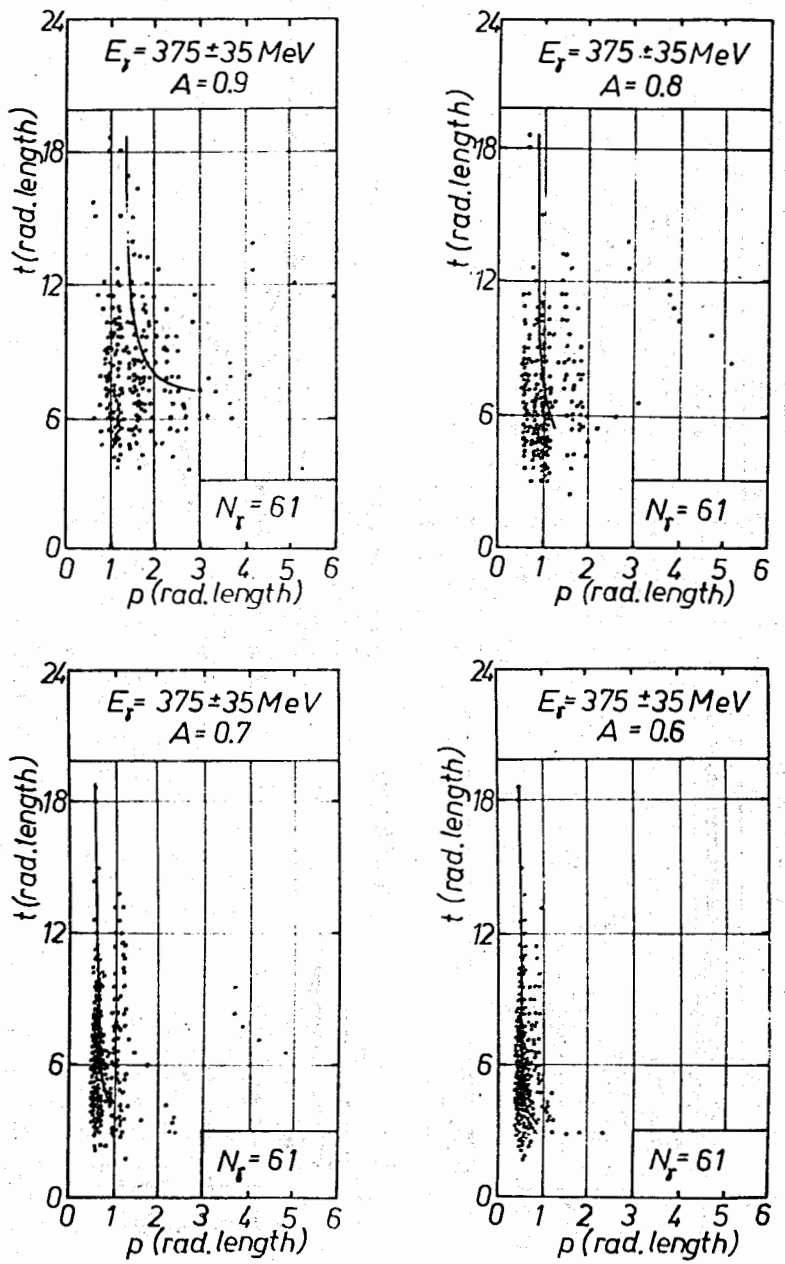


Fig.10. Same as fig.9, for the primary photon energy of 373 ± 35 MeV.

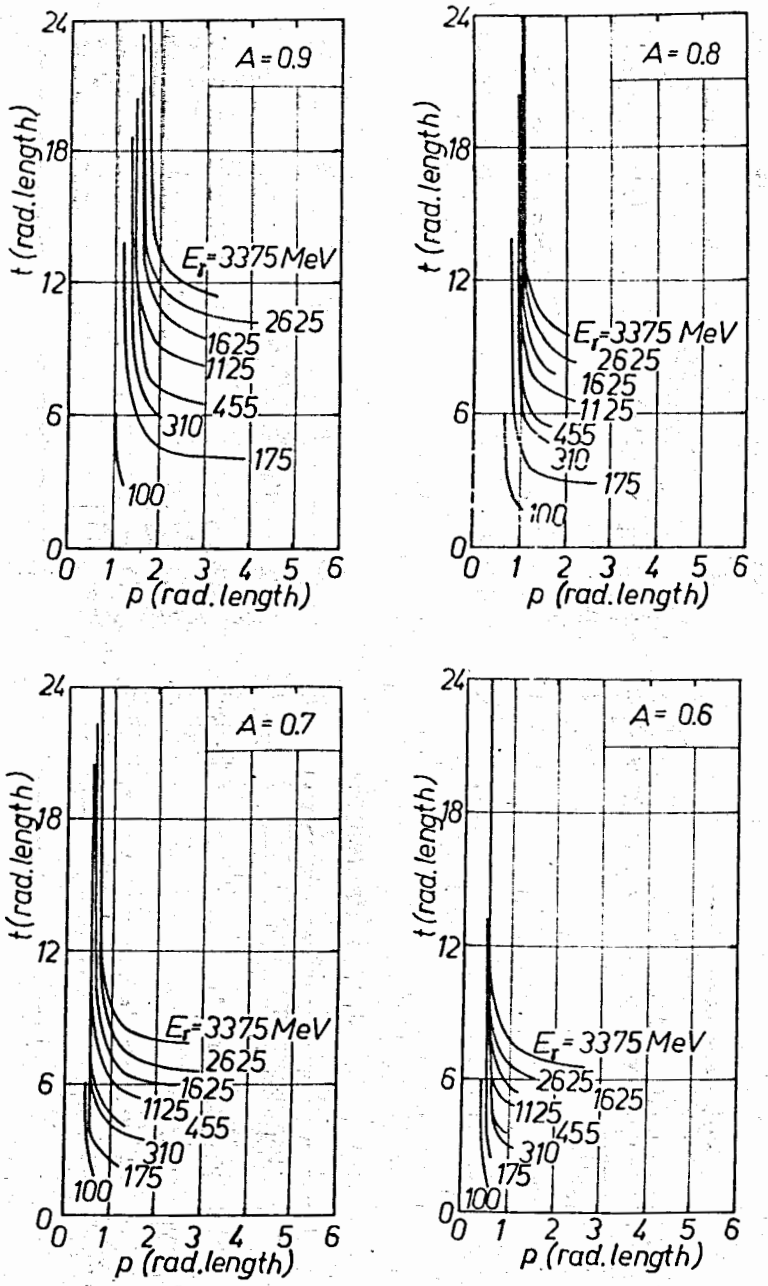


Fig.11. Estimates of average (t vs.p) dependence for different A and $E_\gamma$.



## VII. FLUCTUATIONS

### 1. Longitudinal Fluctuations

Figure 12 shows the standard deviation (SD) $\sigma_A^{(t)}$ of a part A of the IL deposited along the SA as a function of A for six values of energy $E_\gamma$ of shower initiating GQ. One can notice that at $E_\gamma \geq 500$ MeV the behavior of $\sigma_A^{(t)}$ with A is independent of the energy $E_\gamma$, within the experimental error. It was parametrized by a simple parabolic function [18]:

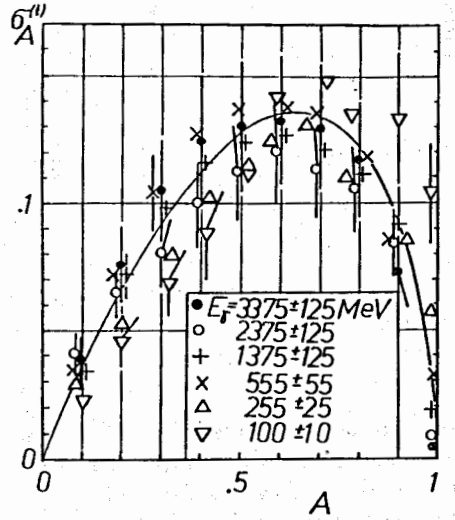


Fig.12. Longitudinal standard deviation of the part A of IL. Solid line displayes the fit to the form (12).

$$\sigma_A^{(t)} = A(\sqrt{\alpha_t^2 + \beta_t(\gamma_t - A)} - \alpha_t) \quad (12)$$

with $\alpha_t = 0.038 \pm 0.001$, $\beta_t = 0.166 \pm 0.005$, $\gamma_t = 1.01 \pm 0.01$, which is illustrated in the figure by the solid curve. It has been found too [14] that A as a random variable meaning the fraction of the total IL at the depth t, where, on the average, the fraction $\bar{A}(t)$ of IL is deposited, obeys the normal distribution with the mean value $\bar{A}(t)$ determined by the probability density function (5) and the dispersion given by eq.(12):

$$A \in N(\bar{A}(t); \sigma_A^{(t)}) \quad (13)$$

at least at $\bar{A}(t) \geq 0.5$.

### 2. Lateral Fluctuations

The lateral fluctuations of IL described by the A dependence of the SD $\sigma_A^{(p)}$ of the part A of the IL measured in the PP as released in the transversal direction away from the SA are shown in Fig.13. They are normalized to the maximum value $(\sigma_{A(\bar{p}_A)})_{max}$ which energy dependence is displayed in Fig.14. and fitted to the linear function of $\ln E_\gamma$ also presented in the figure:

$$(\sigma_{A(\bar{p}_A)}/A)_{max} = \alpha_p - \beta_p \ln E_\gamma, \quad (14)$$

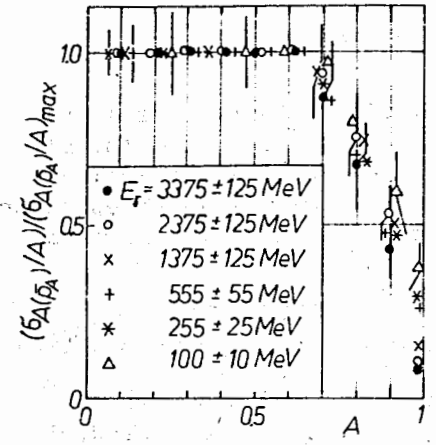


Fig.14. Energy dependence of the maximum lateral standard deviation of the part A of IL.

Fig.13. Lateral standard deviation of the part A of IL normalized to its maximum value.

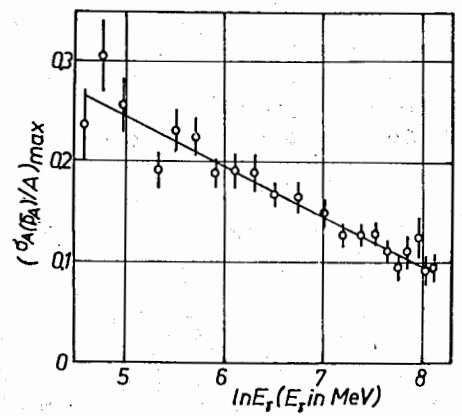


where $\alpha_p = 0.48 \pm 0.02$, $\beta_p = 0.048 \pm 0.003$ and the correlation coefficient r = 0.95.

## 3. Geometric Shape

The longitudinal and transversal shape diffuseness of a shower may be described by the corresponding coefficients of variation $S_t/\bar{t}$ and $S_p/\bar{p}$ which are plotted in Fig.15 for all 22 intervals of energy $E_\gamma$ of shower initiating GQ. Their energy dependence was parametrized by linear functions of $\ln E_\gamma$ as

$$S_t/\bar{t} = A_t - B_t \ln E_\gamma \quad \text{and} \quad S_p/\bar{p} = A_p - B_p \ln E_\gamma, \qquad (15)$$

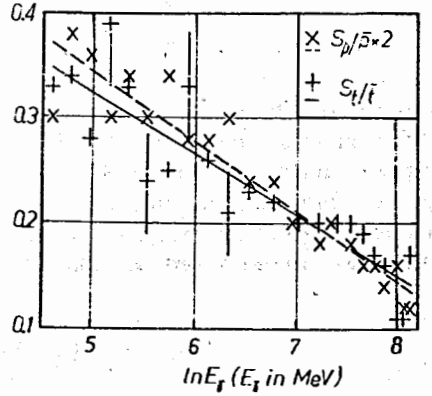


where $A_{t-2} = 0.61 \pm 0.02$, $B_t = (5.8 \pm 0.1) \cdot 10^{-2}$, r = 0.90, and $A_p = 3.38 \pm 0.04$, $B_p = (3.3 \pm 0.1) \cdot 10^{-2}$; r = 0.95. They are showen in the figure as straight lines.

Fig.15. Coefficients of variation of the longitudinal $S_t/\bar{t}$ and the lateral $S_p/\bar{p}$ shower dimensions. Straight lines present the best fits to linear functions (15).



## VIII. CONCLUSIONS

A systematic experimental study of electromagnetic showers produced by GQ of energy $E_\gamma$ = 100-3500 MeV in liquid xenon leads to the following conclusions:

1. The longitudinal distribution of average ionization loss of shower electrons scaled in $\bar{t}(E_\gamma)$ can be described at $E_\gamma \gtrsim$ 500 MeV with good accuracy, by the formula (5).

2. The transversal distribution of average IL, determined as releazed within two parallel planes each being parallel to the shower axis and remote from it by distance p at the depth t, is an exponential function. Integrated over all t it also displayed a simple scaling with the primary GQ energy and material used when expressed in units of average widths $\bar{p}(E_\gamma)$ [19].

3. The depth t and the width p of showers determining some fixed fraction A of their total IL deposited reveal large fluctuations round the relevant average dimensions.

4. Longitudinal fluctuations of IL are described by a simple function of A and are energy independent at $E_\gamma \gtrsim$ 500 MeV. Transversal fluctuations of IL also reveal an approximate scaling with the energy $E_\gamma$ when expressed as a function of A and normalized to their maximum value which logarithmically decreases with increasing GQ energy. Finally, a shower outline detected by means of an ionization effect becomes more and more distinct when the primary photon energy increases.

## REFERENCES


1. Rossi B. - High Energy Particles, Prentice-Hall, 1952.
2. Nelson W.R. - Yoshito Namito. SLAC PUB5193, 9 Febr.1990.
3. Longo E., Sestili I. - Nucl. Instr. and Meth., 1975, 128, p.283.
4. DeAngelis A. - Nucl. Instr. and Metgh., 1988, A271, p.455.
5. Misaki A. - ICR-Report-183-88-29, University of Tokyo, 1988.
6. Okamoto M., Shibata T. - Nucl. Instr. and Meth., 1987, A257, p.155.
7. Grindhammer G., Rudowicz M., Peters S. - Nucl. Instr. and Meth., 1990, A290, p.469.
8. Kuznetsov E.V. et al. - Prib.Tekh.Eksp., 1970, 2, p.56.
9. Niczyporuk B., Słowiński B., Strugalski Z. - JINR, P-2808, Dubna, 1966.
10. Lindblad Th. et al. - Nucl. Instr. and Meth., 1983, 215, p.183.

11. Strugalski Z. - Materials of the Conf. on the Bubble Chamber Techn., JINR, 796, Dubna, 1961.
12. Ivanovskaya I.A. et al. - Prib. Tekh. Eksp., 1968, 2, p.39.
13. Słowiński B., Czyżewska D. - JINR, P13-88-239, Dubna, 1988.
14. Słowiński B. - In: Proc. of the Intern. Meeting of Problems of Mathemat. Simulation in Nuclear Physics Researches, Sept.30-2 Oct., 1980. JINR D10,11-81-622. Dubna, 1981, p.178.
15. Słowiński B. - JINR, E1-89-789, Dubna, 1989.
16. Rust W.W. (Jr.). - Amer. J. Math., 1932, v.54, p.190.
17. Kostritsa A.A. - 87-20, Alma-Ata, 1988.
18. Słowiński B. - JINR, E1-90-274, Dubna, 1990.

Received by Publishing Department
on May 24, 1991.